Theor Appl Climatol (2015) 121:445–458
DOI 10.1007/s00704-014-1249-1

ORIGINAL PAPER

Past and future direct radiative forcing of nitrate aerosol in East Asia

Jiandong Li · Wei-Chyung Wang · Hong Liao · Wenyuan Chang

Received: 10 February 2014 / Accepted: 29 July 2014 / Published online: 14 August 2014

Abstract Nitrate as a rapidly increasing aerosol species in recent years affects the present climate and potentially has large implications on the future climate. In this study, the long-term direct radiative forcing (DRF) of nitrate aerosol is investigated using State Key Laboratory of Numerical Modeling for Atmospheric Sciences and Geophysical Fluid Dynamics (LASG) atmospheric general circulation model (AGCM) and the aerosol dataset simulated by a chemical transport model with focus on East Asia. The DRF due to other aerosols, especially sulfate, is also evaluated for comparisons. Although the chemical transport model underestimates the magnitudes of nitrate and sulfate aerosols when compared with Chinese site observations, some insights into the significances of nitrate climate effects still emerge. The present-day global annual mean all-sky DRF of nitrate is calculated to be −0.025 W m^{-2} relative to the preindustrial era, which is much weaker than −0.37 W m^{-2} for sulfate. However, nitrate DRF may become increasingly important in the future especially over East Asia, given the expectation that decreasing trend in global sulfate continues while the projected nitrate maintains at the present level for a mid-range forcing scenario and even be a factor of two larger by the end of the 21st century for high emission scenarios. For example, the anthropogenic nitrate DRF of −2.0 W m^{-2} over eastern China could persist until the 2050s, and nitrate is projected to account for over 60 % of total anthropogenic aerosol DRF over East Asia by 2100. In addition, we illustrate that the regional nitrate DRF and its seasonal variation are sensitive to meteorological parameters, in particular the relative humidity and cloud amount. It thus remains a need for climate models to include more realistically nitrate aerosol in projecting future climate changes.

J. Li (✉)
State Key Laboratory of Numerical Modeling for Atmospheric Sciences and Geophysical Fluid Dynamics (LASG), Institute of Atmospheric Physics, Chinese Academy of Sciences, 100029 Beijing, China
e-mail: lijd@mail.iap.ac.cn

W.-C. Wang
Atmospheric Sciences Research Center, State University of New York, Albany, NY 12203, USA

H. Liao · W. Chang
State Key Laboratory of Atmospheric Boundary Layer Physics and Atmospheric Chemistry (LAPC), Institute of Atmospheric Physics, Chinese Academy of Sciences, 100029 Beijing, China

J. Li
Collaborative Innovation Center on Forecast and Evaluation of Meteorological Disasters, Nanjing University of Information Science and Technology, 210044 Nanjing, China

1 Introduction

Aerosols can influence the Earth's radiation budget directly by scattering and absorbing solar radiation and indirectly by serving as cloud condensation nuclei to alter cloud optical properties and precipitation processes. The atmospheric loading of anthropogenic aerosols has increased distinctly due to economic and agriculture activities since the preindustrial era (PI). Unlike well-mixed greenhouse gases (GHGs), the global mean radiative forcing (RF) by anthropogenic aerosols is estimated to have a net cooling effect, with RF values of −0.35 W m^{-2} (range −0.85 to +0.15) for direct effects and −0.45 W m^{-2} (range −1.2 to 0.0) for indirect effects (Myhre et al. 2013a). In particular, aerosol effects in some industrialized regions are much higher than the global mean. Of the anthropogenic aerosols, sulfate is considered to be the largest contributor, the RF and climate effects of which have been widely investigated (Schulz et al. 2006; Myhre et al. 2013b). However, sulfate emissions and atmospheric concentrations started to continuously decrease over many regions, such as Europe and North America, since the 1980s (Folini and Wild 2011; Smith et al. 2011). Moreover, some recent studies (Takemura 2012; Shindell et al. 2013) suggest that aerosol

RF has peaked and is projected to reach a much lower level by 2100 relative to the present day (PD). It seems that sulfate RF becomes increasingly weak relative to the warming effect of GHGs. This is not the case for nitrate aerosol. Nitrate is an important rapidly increasing species in recent years and is expected to become more important as a climate forcing factor due to the anticipated increases in nitrate precursor emissions and the decline of ammonium sulfate (Adams et al. 2001; Bauer et al. 2007). Observations have shown that concentrations of nitrate even exceed those of sulfate over some European regions (Schaap et al. 2004). The nitrate loading is also very high over eastern China (Wang et al. 2010; Zhang et al. 2012a). The projected RF due to nitrate aerosol even exceeds sulfate aerosol by the end of the 21st century (Liao and Seinfeld 2005; Bellouin et al. 2011). In addition to the differences in emissions and long-term trends, nitrate formation processes also differ from sulfate. For example, low temperatures favor nitrate formation but can result in decreases in gas-phase reaction rates and oxidant concentrations associated with sulfate formation (Pathak et al. 2004). The seasonal changes in mass concentrations of these two aerosol species are therefore different over some regions. Hence, examining nitrate RF and its possible time evolution is very important for quantifying anthropogenic climate change.

Although some studies have investigated nitrate indirect effects (e.g., Xu and Penner 2012), most previous studies focused on nitrate direct radiative forcing (DRF). Even so, not enough attentions have been paid to nitrate aerosol in climate models. For example, nitrate was not included in phase 1 of the Aerosol Comparisons Between Observations and Models (AeroCom) project (Schulz et al. 2006), and only half of the climate models involved in AeroCom II take into account nitrate aerosol. In fact, present model estimations with regard to nitrate DRF still demonstrate a large spread. The global multi-model mean nitrate DRF according to Myhre et al. (2013b) varies from −0.12 to −0.02 W m^{-2}, while the results in Shindell et al. (2013) range from −0.41 to −0.03 W m^{-2}. The more recent estimation by Myhre et al. (2013a) gives a median value of −0.11 W m^{-2}, ranging from −0.30 to −0.03 W m^{-2} for anthropogenic nitrate DRF. As for the global and regional time evolution of nitrate DRF, only a limited number of studies have investigated historical time series (e.g., Skeie et al. 2011) and the projected change (e.g., Bellouin et al. 2011) regarding nitrate loading and DRF. Also, few of existing studies are aimed specially at long-term variation of nitrate DRF in East Asia. It is well known that both regional air quality and climate are strongly affected by high aerosol concentrations in China (Li et al. 2010; Sun et al. 2014), where nitrate is an important aerosol species. It is therefore essential to further examine East Asian nitrate DRF and its possible time evolution.

The aim of this study is to investigate the time evolution of nitrate DRF with an atmospheric general circulation model (AGCM) and a long-term aerosol dataset taken from National Center for Atmospheric Research Community Atmosphere Model with Chemistry (NCAR CAM-Chem) (Lamarque et al. 2012). The historical and projected changes in nitrate DRF are examined for the global and selected regional domains, and our emphasis is on East Asia. In our work, sulfate loading and DRF are as contrast results to show the importance of nitrate. Meanwhile, relative contribution from nitrate to anthropogenic aerosol DRF is examined. We also analyze the effects of simulated regional climate characteristics including relative humidity (RH) and clouds on present seasonal variation of nitrate DRF over East Asia, Europe, and North America. Owing to considerable uncertainties associated with nitrate aerosol, some in situ aerosol measurements in China are used to compare with model results in order to discuss the possible uncertainties in estimating nitrate DRF. The remainder of the paper is organized as follows. Section 2 introduces the dataset and methodology used in the study. Section 3 presents the major results. Section 4 gives the conclusions and a brief discussion.

2 Model description, dataset, and experimental design

To calculate the instantaneous aerosol RF, meteorological fields are simulated by the AGCM. The AGCM used in this study is developed by the State Key Laboratory of Numerical Modeling for Atmospheric Sciences and Geophysical Fluid Dynamics (LASG), Institute of Atmospheric Physics (IAP), Chinese Academy of Sciences. It has 26 vertical hybrid layers, and its horizontal resolution is approximately 2.81° longitude × 1.67° latitude. The model is able to reproduce the mean large-scale climate patterns and climate variability at various timescales and has been used in many studies (e.g., Wu et al. 2012; He et al. 2013). For more details, readers are referred to the paper by Bao et al. (2013). The radiation scheme (Sun and Rikus 1999; Sun 2011) used in the AGCM is modified from that developed by the UK Meteorological Office (Edwards and Slingo 1996; Martin et al. 2006) based on the two-stream equation approach. The scheme utilizes a correlated k-distribution method (Fu and Liou 1992; Mlawer et al. 1997; Li and Barker 2005) and can simulate major gaseous absorption due to water vapor, carbon dioxide, ozone, methane, nitrous oxide, oxygen, and chlorofluorocarbons (Sun 2011). The treatment of cloud optical properties (Hu and Stamnes 1993; Chou 2002) is included in the radiative scheme.

The long-term three-dimensional monthly mean aerosol fields are taken from the simulation from the NCAR CAM-Chem (Lamarque et al. 2011, 2012), and major anthropogenic species include black carbon (BC), nitrate, organic carbon (OC), and sulfate. Nitrate and sulfate compositions are represented as ammonium nitrate (NH_4NO_3) and ammonium sulfate ($(NH4)_2SO_4$), respectively. The dataset covers the period from the 1850s to 2100, and each 10-year set of results is averaged to produce the decadal mean. The decades of 1850–1859 and 2000–2009 represent the PI and PD, respectively.

There are four Representative Concentration Pathway (RCP) scenarios for the period 2010–2100 (Vuuren et al. 2011). Our focus is on future increasing emission scenarios, and so the middle (RCP4.5), higher (RCP6.0), and highest (RCP8.5) scenarios are used in this study. The anthropogenic aerosols and the associated DRF are estimated as the differences between a specified decade and the PI.

The aerosol RF is obtained using a "double radiation call" method, in which the radiation scheme is called twice at each radiation time step (3 h). In the first call, no aerosol species are used; in the second call, aerosol loading at a specified decadal is used, and aerosols only affect the radiative process without influencing other climate processes. The meteorological variables are the same for the two calls. The difference in radiative fluxes at the top of atmosphere (TOA) during the two calls is determined to be the RF during a specified period due to aerosols. The GHGs, ozone, and solar forcing are fixed at present levels using the Coupled Model Intercomparison Project phase 5 (CMIP5) dataset (Taylor et al. 2012). The sea surface temperature and sea ice are from the prescribed Atmospheric Model Intercomparison Project (AMIP) climatology.

In the NCAR CAM-Chem dataset, only the bulk mass is calculated, and the lognormal distribution is assumed for anthropogenic aerosol species. According to original NCAR aerosol dataset and some relevant work (e.g., Kiehl et al. 2000; Liao et al. 2004), aerosol physical parameters are chosen. The nitrate DRF was calculated with sulfate optics in some previous studies. This treatment is prone to underestimating the magnitude of nitrate DRF because the extinction ability for nitrate is generally stronger than sulfate (Fitzgerald 1975; Zhang et al. 2012b). In our study, optical properties of nitrate and sulfate aerosols are calculated separately. The refractive indices of dry nitrate and sulfate are from Toon et al. (1976) and the Global Aerosol Climatology Project Database (http://gacp.giss.nasa.gov/data_sets), respectively; the refractive indices of dry BC and OC are based on Haywood and Ramaswamy (1998) and Hess et al. (1998), respectively. BC is treated as dry aerosol. The variations of optical properties of nitrate and sulfate aerosols with RH (hydroscopic effects) follow the work of Li et al. (2001, 2012) and those of OC follow the treatment of Hess et al. (1998). These aerosol optical properties are then obtained with Mie calculations, assuming that aerosol species are externally mixed. Table 1 presents aforementioned physical parameters and optical properties at 0.55 μm for aerosols used in this study.

Table 1 Physical parameters and optical properties at 0.55 μm for BC, nitrate, OC, and sulfate aerosols

	Refractive index	r_g	σ	ρ	σ_e	ω	g
BC	1.75−0.44 i	0.0118	2.00	1.0	9.26	0.21	0.34
OC	1.53−0.006 i	0.0212	2.24	1.8	2.91	0.96	0.61
Nitrate	$1.56-1.1\times10^{-9}\ i$	0.0500	2.00	1.700	3.98	1.0	0.63
Sulfate	$1.53-1.0\times10^{-7}\ i$	0.0500	2.00	1.769	3.41	1.0	0.64

Here, r_g geometric radius (μm), σ standard deviation (μm), ρ mass density (g cm^{-3}), σ_e extinction coefficient (m^2 g^{-1}), ω single-scattering albedo, g asymmetry factor

3 Results

3.1 Global distribution of present nitrate DRF

Figure 1 shows the global distributions of anthropogenic nitrate loading, aerosol optical depth (AOD), and DRF in the 2000s relative to the PI. Here, the AOD is the averaged value for the band of 0.50–0.625 μm. In the Northern Hemisphere, the stronger nitrate loading is distributed in industrialized regions including North America, Europe, and South and East Asia. The maximum loading in Central Europe and East China is even over 5 mg m^{-2} and quite stronger than the global mean value of 0.15 mg m^{-2}. The spatial patterns of nitrate AOD and DRF are roughly consistent with its loading, but the clear-sky nitrate DRF is stronger than its all-sky DRF because of the blocking effects of clouds (Takemura et al. 2002; Zhang et al. 2012c). The global mean anthropogenic nitrate TOA DRF is calculated to be −0.046 and −0.025 W m^{-2} for clear and all-sky conditions, respectively. The nitrate all-sky DRF in our study is within the range of present multi-model estimations by Forster et al. (2007) and Myhre et al. (2013b) but is somewhat lower than many of model results in the two studies as given here. This is partly because the input nitrate loading in our work is in the lower end of the multi-model estimates (0.14 to 0.90 mg m^{-2}) summarized by Myhre et al. (2013b). Besides, only the bulk nitrate loading is used in our calculation, and the contribution of fine-mode (<0.05 μm) nitrate to its extinction is not well considered. This is another cause leading to the relatively weaker all-sky nitrate DRF in our work. If the nitrate DRF is normalized by the loading, the normalized DRF (NDRF) value of −167 W g^{-1} is very close to the recent multi-model median value of −166 W g^{-1} by Myhre et al. (2013b). This shows that the calculated nitrate optical properties are comparable to those in many climate models although relatively weaker nitrate loading is applied in this study.

3.2 Time evolution of nitrate loading and DRF

Figure 2a, b shows time series of anthropogenic sulfate and nitrate loadings relative to the PI. According to the present distribution of nitrate loading as shown in Fig. 1a, we choose three major industrialized regions including East Asia, Europe, and North America to examine the regional mean time evolution. The regional domains are given in the figure caption. There is a remarkable increase for nitrate and sulfate

Fig. 1 The global annual mean anthropogenic nitrate **a** atmospheric loading (mg m^{-2}), **b** aerosol optical depth at 0.50–0.625 μm, **c** DRF (W m^{-2}) at clear-sky TOA, and **d** DRF (W m^{-2}) at all-sky TOA in the 2000s relative to the PI (1850s)

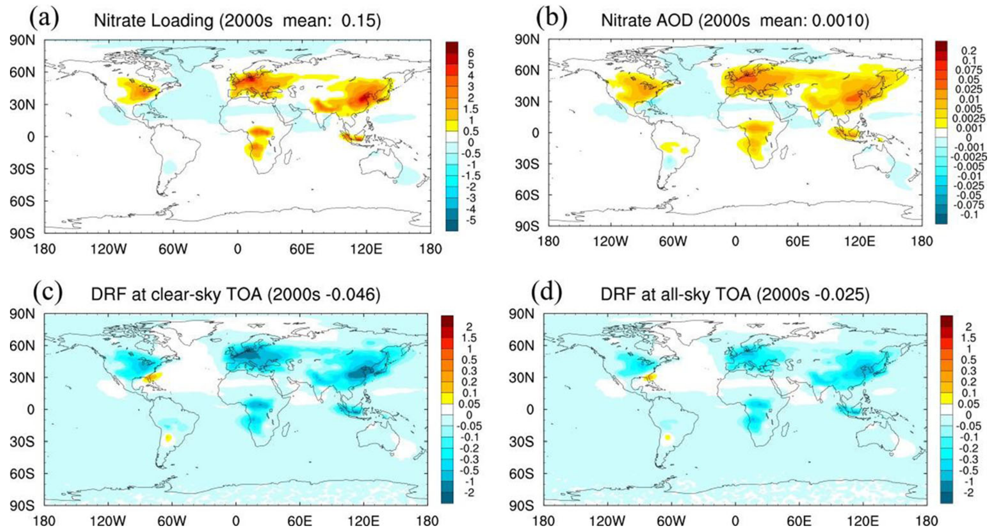

loadings since the 1950s. In Europe and North America, the sulfate loading peaks in the 1970s. In East Asia, the sulfate loading is projected to increase until the 2010s under RCP4.5 and RCP8.5 scenarios, but large sulfate loading may even continue until the 2050s under the worst-case scenario, RCP6.0. However, according to the RCP scenarios, the sulfate loading over all of these regions is projected to decrease to, or fall below, the PI level by 2100. Similar results are also reported by Takemura (2012) for sulfate and carbonaceous aerosols. In contrast to sulfate aerosol, the global mean nitrate loading is projected to remain the same under RCP4.5 until year 2100 and may even increase to higher levels under RCP6.0 and RCP8.5. Meanwhile, the nitrate loading in major industrialized regions is much stronger than the global mean. The projected maximum nitrate loading in East Asia is much larger than that in Europe or North America. The nitrate loading over East Asia peaks in the 2030s under RCP4.5 and RCP8.5 and in the 2050s under RCP6.0.

The time evolution of sulfate and nitrate DRF at all-sky TOA is similar to their loading change. As presented in Fig. 2d, the global and regional averaged nitrate DRFs increase since the PI. After the 1980s, the nitrate DRF over East Asia exceeds that in Europe and becomes the largest contributor among the three regions. It should be noted that the worst-case future scenario for East Asia is RCP6.0, under which the nitrate DRF peaks in the 2050s with a value of −0.547 W m^{-2}, which is much higher than the peak values of over the other two regions. The peak periods and magnitudes of nitrate DRF are summarized in Table 2. The results presented here indicate that the DRF due to nitrate aerosol, especially in East Asia,

Fig. 2 Time series of **a** sulfate atmospheric loading (mg m^{-2}), **b** nitrate atmospheric loading (mg m^{-2}) and **c** sulfate and **d** nitrate DRFs (W m^{-2}) at all-sky TOA. Here, the period is relative to the PI. Domain mean values are global (*GL*), and for East Asia (*EA* 20–45° N, 100–145° E), Europe (*EU* 35–60° N, 0–45° E), and North America (*NA* 25–50° N, 245–290° E) for the historical period and projected future (since the 2010s). “45,” “60,” and “85” denote the RCP4.5, RCP6.0, and RCP6.0 scenarios, respectively

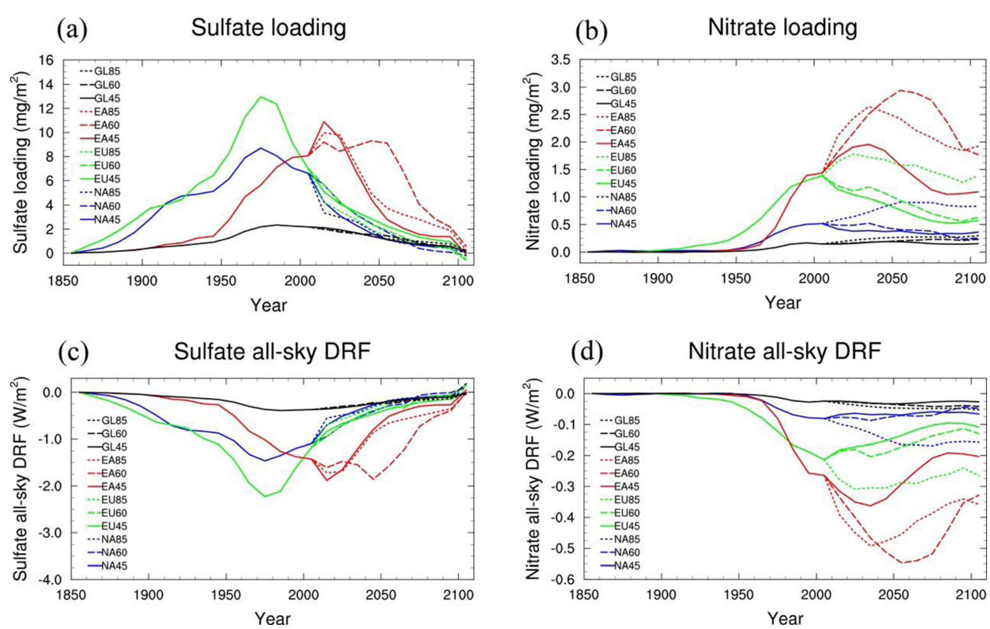

Table 2 Peak times and magnitudes of global and regional nitrate DRFs (W m^{-2})

	Hindcast	RCP4.5	RCP6.0	RCP8.5
Global	–	(2040s, −0.033)	(2070s, −0.042)	(2100, −0.053)
East Asia	–	(2030s, −0.363)	(2050s, −0.547)	(2030s, −0.493)
Europe	(2000s, −0.213)	–	–	(2020s, −0.308)
North America	(2000s, −0.081)	–	(2030s, −0.087)	(2070s, −0.169)

If the maximum value occurs under the projected scenario, the decade in which the maximum occurs and the value are shown; otherwise, the maximum occurs in the historical period

will become an increasingly important component of RF due to anthropogenic aerosols in the remaining part of the 21st century.

To further examine the global changes in projected nitrate all-sky DRF, three decadal results under different RCPs are given in Fig. 3 to illustrate the future changes relative to the PD. The selected decades are the 2030s, 2050s, and 2090s, representing the early, middle, and end of the 21st century, respectively. Under the middle-range RCP4.5, an evident decrease in nitrate DRF appears over Europe and North America, and the decrease is more significant in the 2090s, when the global mean projected nitrate DRF is reduced to the PD level. However, large increases in nitrate DRF still occur over Asian regions under RCP4.5 until the 2050s, when increased DRF is even up to −2.0 W m^{-2} over East Asia. Under more severe RCP6.0 and RCP8.5 scenarios, the global mean nitrate DRF is intensified at the global scale, and the projected global mean nitrate DRF increases by 56 and 96 %, respectively, in the 2090s relative to PD. Under RCP8.5, the negative DRF over most regions remains between the 2050s and 2090s. It should be noted in Fig. 3 that the worst nitrate RF in East Asia is projected to occur in the 2050s under RCP6.0, rather than RCP8.5, and the reduced DRF relative to the PD could be up to −1.0 W m^{-2} (namely, over −2.0 W m^{-2} DRF relative to the PI). This indicates that the RCP6.0 scenario is representative of a far worse future in some regions, such as East Asia, although RCP8.5 generally leads to stronger nitrate DRF at the global scale.

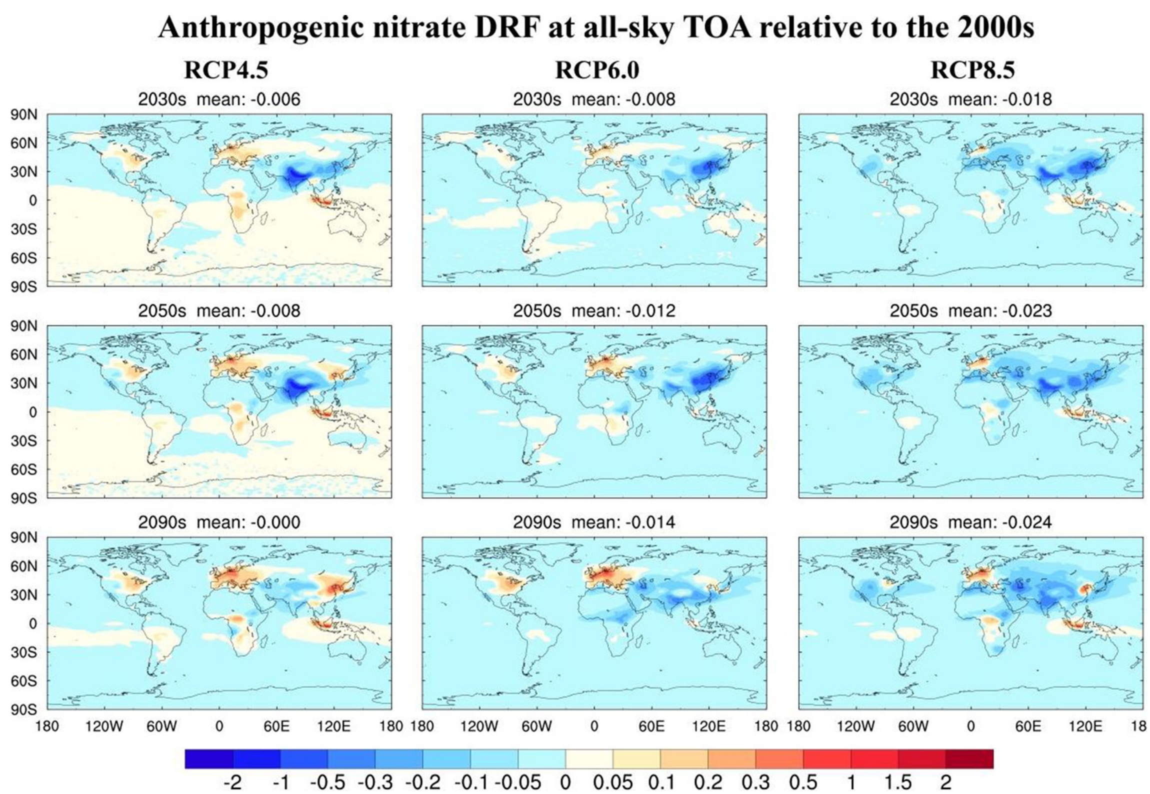

Fig. 3 Nitrate DRF (W m^{-2}) at all-sky TOA in the 2030s (*upper row*), 2050s (*middle row*), and the 2090s (*bottom row*) relative to the PD (2000s). The *left*, *middle*, and *right columns* are for the RCP4.5, RCP6.0, and RCP8.5 scenarios, respectively. The global mean values are shown at the *top of each panel*

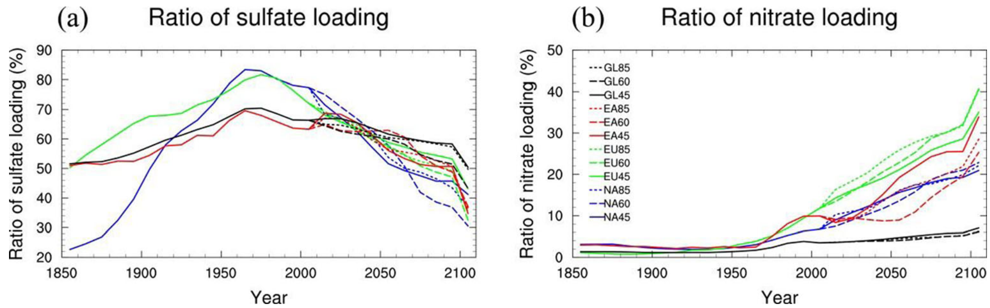

Fig. 4 Time series of the ratio of **a** sulfate and **b** nitrate loadings to total aerosol loading excluding dust and sea-salt aerosols. Here, the loading resources include anthropogenic and natural aerosols

3.3 The contribution of nitrate to anthropogenic aerosol DRF

To investigate the relative importance of nitrate among anthropogenic aerosols, we calculate the ratios of sulfate and nitrate loadings to four aerosol species including BC, nitrate, OC, and sulfate, which are mainly from anthropogenic sources. These aerosol loadings are from both anthropogenic and natural resources. In Fig. 4, similar to the evolution of loading examined above, the global and regional sulfate loading ratios exhibit increases since the PI. The present global mean sulfate ratio is about 66 %, and the ratio in Europe and North America is even up to 80 %. However, the sulfate loading ratio is projected to decrease to be about 50 % on the global scale, and the ratios are about 40 % in the three regions by 2100. On the contrary, the global and regional nitrate ratios show a continuously increasing trend. In particular, the projected nitrate ratios in East Asia and Europe are up to 30 % by 2100. This indicates that the nitrate loading is close

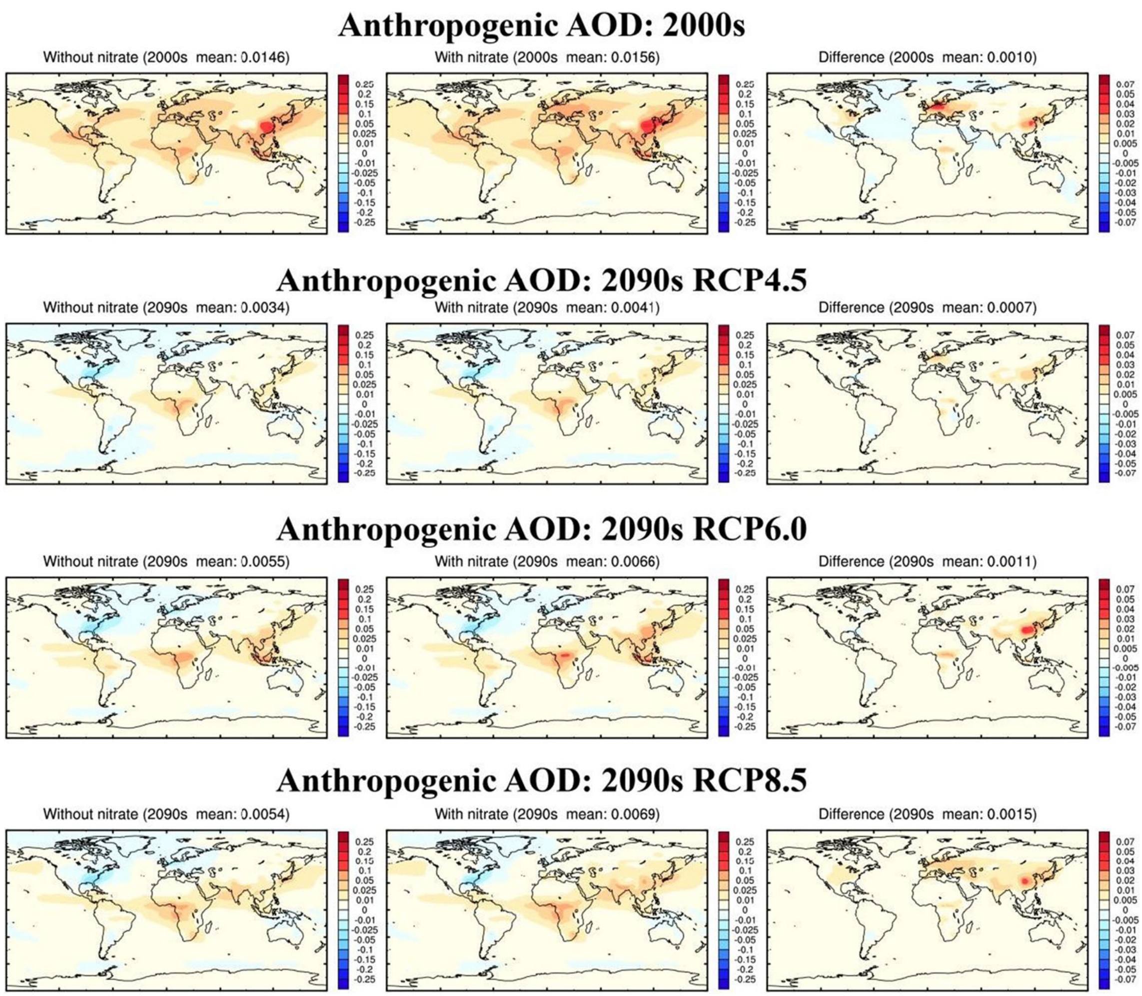

Fig. 5 The global distributions of anthropogenic aerosol AOD at 0.50–0.625 μm relative to the PI (1850s) for the 2000s (*first row*) and 2090s under RCP4.5 (*second row*), RCP6.0 (*third row*), and RCP8.5 (*fourth row*). The *left* and *middle columns* are for excluding and including nitrate aerosols, respectively, and the *right column* is for their difference

to those of sulfate aerosol by the end of the 21st century. Thus, the gradually increasing ratio of nitrate mass to anthropogenic aerosols under future scenarios shows that nitrate will play more important roles in future aerosol AOD and RF, especially at regional scales.

Figure 5 shows the global distribution of anthropogenic aerosol AOD in the 2000s and 2090s relative to the PI, with and without nitrate and differences due to nitrate. In the 2000s, large anthropogenic AOD is over Central and Eastern Northern America, Europe, and East Asia, and the largest value occurs in the eastern China. When nitrate is included, increased AOD is mainly located in the Eastern USA, Europe, and eastern China. The negative AOD over some regions arises from decreased nitrate loading relative to the PI. These results are also agreement with the distribution of nitrate loading and AOD as shown in Fig. 1. In the 2090s, anthropogenic AOD under three future scenarios is much reduced over Northern America and Europe, but the AOD caused by nitrate still increases over Northern Hemispheric regions, such as eastern China and South Asia. It is seen from the differences in AOD that nitrate aerosol contributes a large fraction of anthropogenic AOD over East Asia in the 2090s. After the inclusion of nitrate aerosol, the global mean anthropogenic AODs increase by 7.53 % for the 2000s and 20.59, 20.00, and 27.78 % for the 2090s under RCP4.5, RCP6.0, and RCP8.5, respectively.

As shown in Figs. 6 and 7, when nitrate is considered, the present anthropogenic aerosol DRF at TOA is calculated to be −0.632 and −0.269 W m^{-2} for clear-sky and all-sky, respectively. Our estimates are close to the estimates of anthropogenic aerosol DRF by Mythre et al. (2013b) for clear-sky (model mean −0.67 W m^{-2}; range −1.01 to −0.35 W m^{-2}) and all-sky (model mean −0.27 W m^{-2}; range −0.58 to −0.02 W m^{-2}). Meanwhile, the global patterns of anthropogenic aerosol DRF are similar to those of anthropogenic AOD. In the 2000s, nitrate contributes up to −1.0 W m^{-2} over Northern Hemispheric industrialized regions at the clear-sky TOA. In the 2090s, the inclusion of nitrate makes large anthropogenic aerosol DRF over

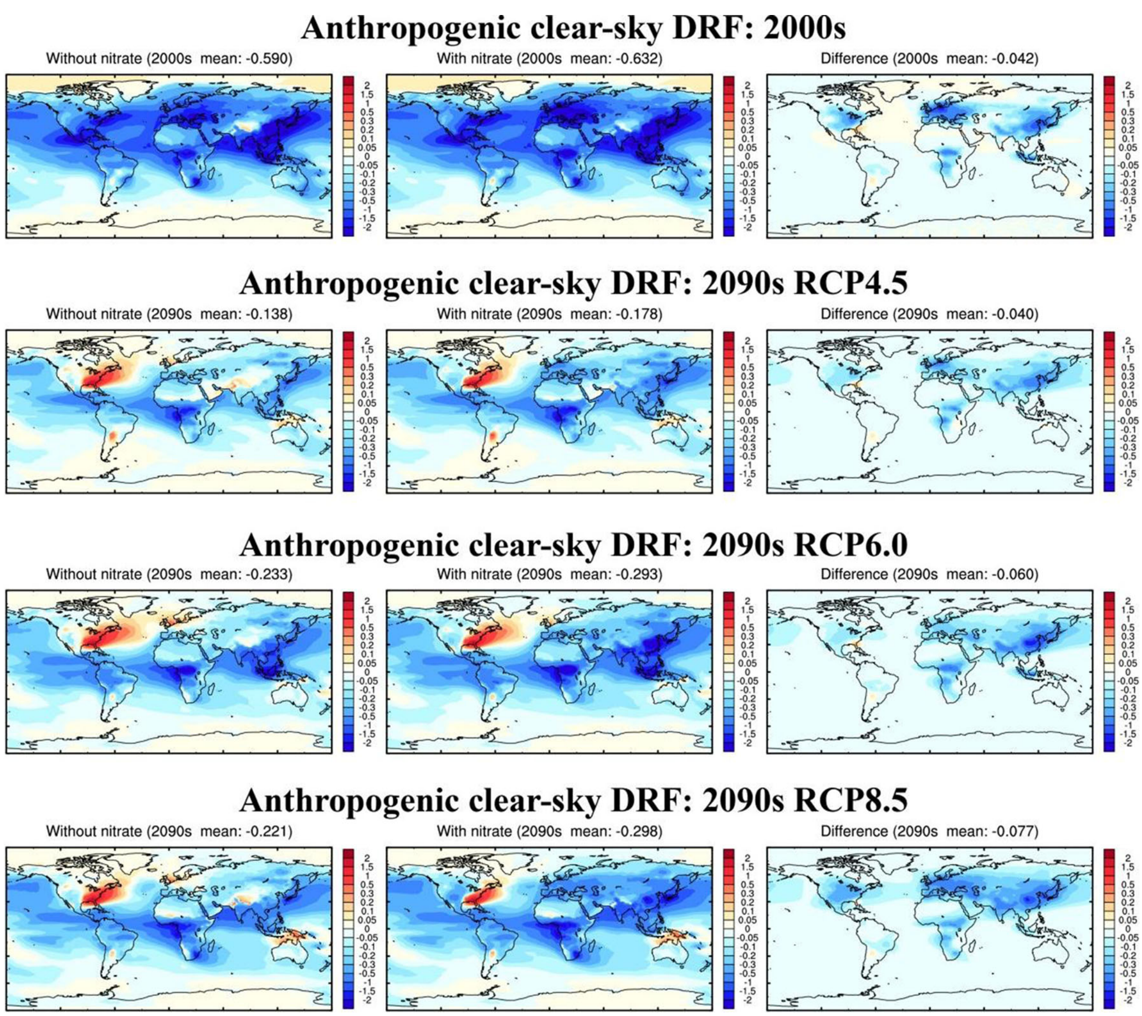

Fig. 6 Same as Fig. 5 but for anthropogenic aerosol DRF (W m^{-2}) at clear-sky TOA

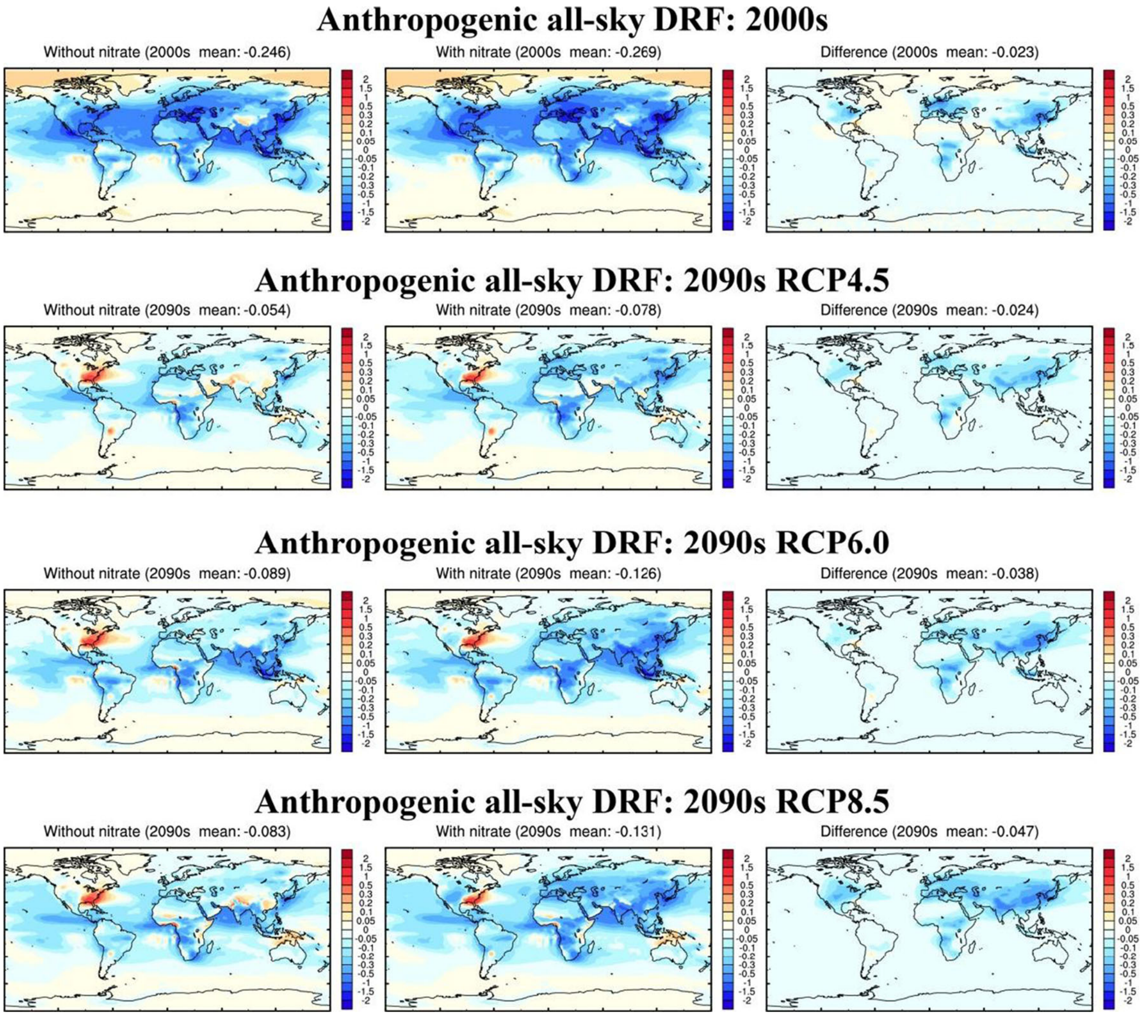

Fig. 7 Same as Fig. 5 but for anthropogenic aerosol DRF (W m^{-2}) at all-sky TOA

Northern America, Europe, and East Asia remaining in the 2000s level. With regard to the global scale, nitrate leads to increases in the global mean clear-sky TOA anthropogenic aerosol DRF by 7.12 % in the 2000s and by 28.59, 25.75, and 34.84 % in the 2090s under RCP4.5, RCP6.0, and RCP8.5, respectively. In all-sky condition, the corresponding increases in anthropogenic aerosol DRF due to nitrate are 9.35, 44.44, 42.70, and 56.63 %.

The above results indicate that nitrate aerosol has important contributions to the global mean anthropogenic AOD and aerosol DRF. In particular, compared to the global scale, the role of nitrate in anthropogenic aerosol DRF is more significant over East Asia due to the relatively higher regional loading. So, time series of anthropogenic aerosol AOD and DRF over East Asia are shown in Fig. 8 together with the nitrate ratios. Because the nitrate loading over East Asia rapidly increases since 1950 (as given in Fig. 2), the period chosen here is from 1950 to 2100. With the increasing ratio of nitrate loading to anthropogenic aerosol species since 1950, the anthropogenic aerosol AOD and DRF with nitrate are clearly larger than those without nitrate. The biggest contribution of nitrate is projected to occur under the RCP6.0 during 2050 to 2070, when nitrate aerosol contributes about −0.90 and −0.51 W m^{-2} over East Asia, respectively. Furthermore, as shown in Fig. 8d–f, the ratios of AOD and DRF from nitrate to the total anthropogenic AOD and DRF gradually increase except for several decades under RCP4.5 all-sky condition. By the end of the 21st century, the projected ratio of nitrate can reach 0.40 for total anthropogenic aerosol AOD and clear-sky DRF and is even over 0.60 for all-sky DRF. As mentioned above, clouds can reduce aerosol TOA DRF by scattering aerosols. Consequently, aerosol DRF at all-sky TOA is much reduced, and then, higher contribution ratio of nitrate appears in all-sky condition. The quantitative contributions of nitrate aerosol at the global scale and East Asia in the 2000s and 2090s are summarized in Table 3. The analysis presented in our work shows that nitrate is estimated to the biggest contributor to total anthropogenic aerosol DRF in East Asia by the end of the 21st century. Hence, nitrate aerosol should

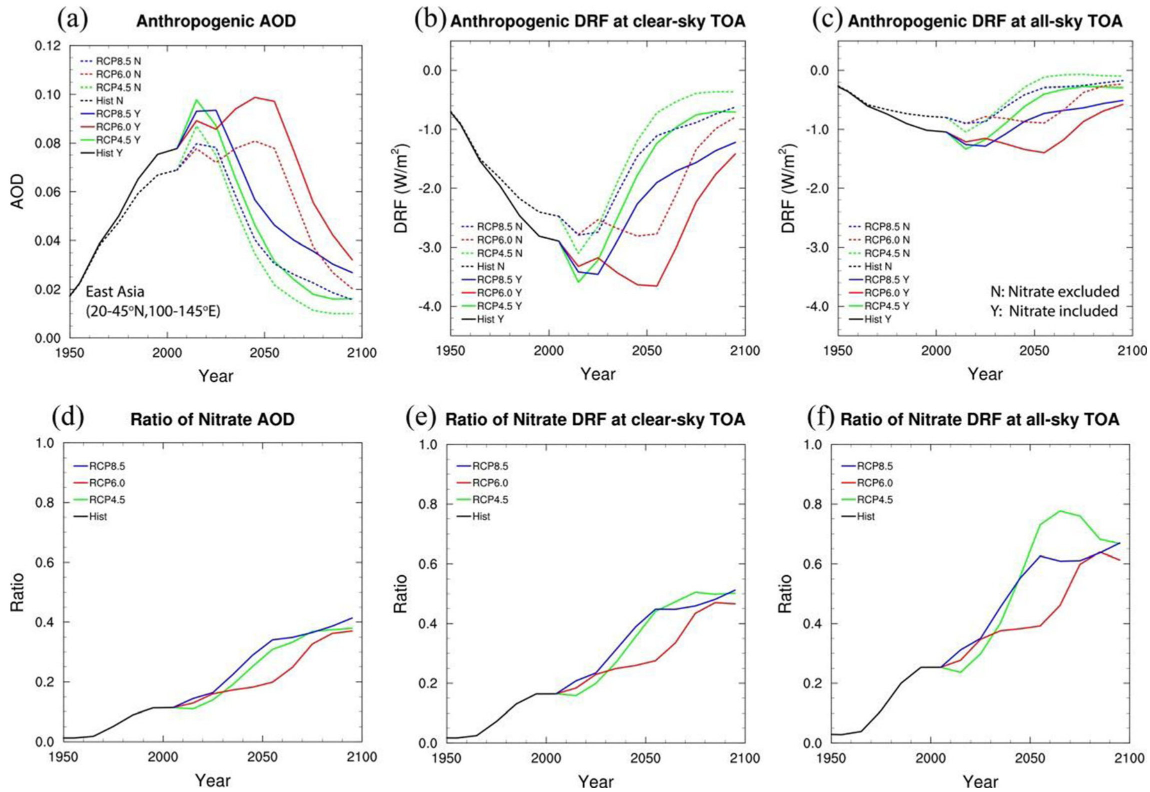

Fig. 8 Time series of total anthropogenic aerosol **a** AOD, **b** DRF (W m^{-2}) at clear-sky TOA, and **c** DRF (W m^{-2}) at all-sky TOA; ratio of nitrate **d** AOD, **e** DRF (W m^{-2}) at clear-sky TOA, and **f** DRF (W m^{-2}) at all-sky DRF to total anthropogenic aerosol AOD over East Asia. Here, AOD is at 0.50–0.625 μm. *Solid lines* include nitrate aerosol and *dashed lines* do not

be paid more attentions in the future studies associated with aerosol climate effects.

3.4 Seasonal cycle of present nitrate DRF

Figure 9 shows seasonal cycles in nitrate loading, AOD, and DRF in the 2000s derived from the difference between experiments with and without nitrate. Nitrate loading, AOD, and DRF show distinct seasonal variations, and their maximum values occur in winter when low temperatures favor nitrate formation, and hence, nitrate loading is the largest. In January, the heaviest nitrate loading is over East Asia, but the nitrate AOD and clear-sky DRF over Europe are larger than those over East Asia although the latter has the heaviest nitrate loading. In addition to atmospheric loading, key regional meteorological factors including relative humidity (RH) and clouds also strongly modulate the magnitude of aerosol DRF and its distribution. To examine the above issues, we present seasonal changes in simulated surface RH and total cloud over three regions in Fig. 10. The highest near-surface RH in January occurs over Europe and is even up to 80 %. High RH is helpful to enhance the hygroscopic effect of hydrophilic nitrate aerosol and increase aerosol extinction. As a result, the nitrate AOD and clear-sky DRF over Europe are larger than

Table 3 Anthropogenic nitrate and total aerosol DRF and nitrate ratios at all-sky TOA in the 2000s and 2090s under three scenarios

	Global all-sky TOA			East Asian all-sky TOA		
	Nitrate DRF (W m^{-2})	Total DRF (W m^{-2})	Ratio (%)	Nitrate DRF (W m^{-2})	Total DRF (W m^{-2})	Ratio (%)
2000s	−0.025	−0.269	9.29	−0.264	−1.043	25.32
2090s						
RCP4.5	−0.025	−0.078	32.05	−0.195	−0.292	66.73
RCP6.0	−0.039	−0.126	30.95	−0.353	−0.576	61.30
RCP8.5	−0.048	−0.131	36.64	−0.340	−0.508	66.93

Here, ratio is the only value with nitrate to the total anthropogenic aerosol DRF due to BC, nitrate, OC, and sulfate. The anthropogenic values are relative to the PI (1850s)

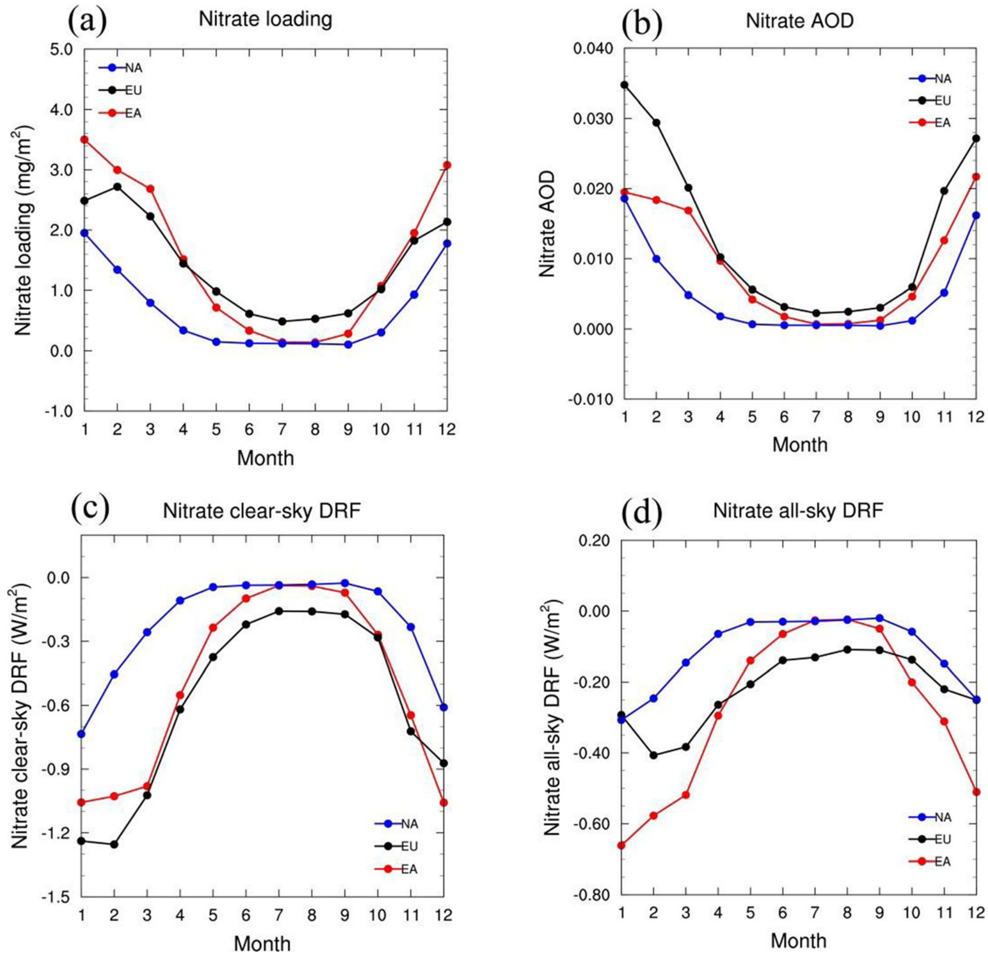

Fig. 9 Seasonal cycle of nitrate **a** atmospheric loading (mg m^{-2}), **b** AOD, **c** clear-sky DRF, and **d** all-sky DRF in the 2000s. Here, AOD is the average value for the band 0.50–0.625 μm, and the nitrate DRF is derived from the experiments with and without nitrate

those over East Asia. The situation is different in all-sky conditions during winter, where all-sky DRF in East Asia is much stronger than in Europe, because the simulated cloud fraction in the latter is larger than the former.

The results given above show that regional aerosol DRF and their seasonal variations are not only affected by its loading but also modulated by the simulated meteorological fields. It should be noted that meteorological fields in this study are simulated from our AGCM and are somewhat inconsistent with the aerosol fields from NCAR CAM-Chem. In this situation, the inherent connections between aerosol, RH, and clouds are not reflected in our calculation. In fact, similar inconsistencies between meteorological and aerosol datasets are common in numerous climate simulations, for example, the CIMIP5 simulations as described by Taylor et al. (2012). We further discuss relevant issues in Sect. 4.

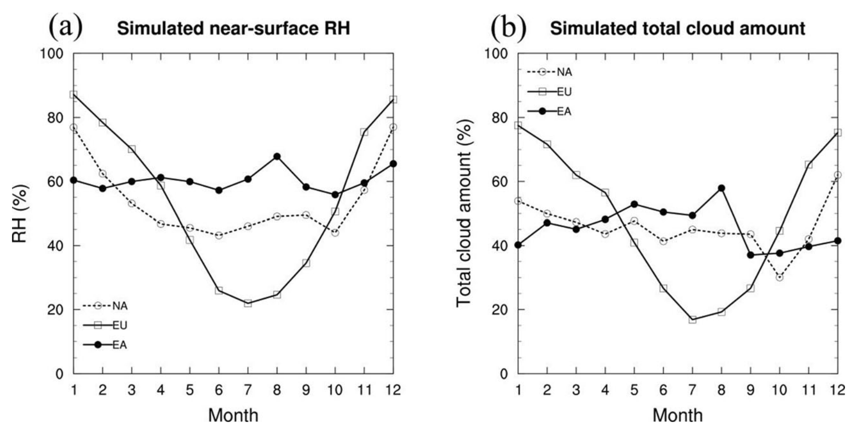

Fig. 10 Seasonal cycle of simulated near-surface RH (%) and total cloud amount over the three regions. The domains are the same as in Fig. 2

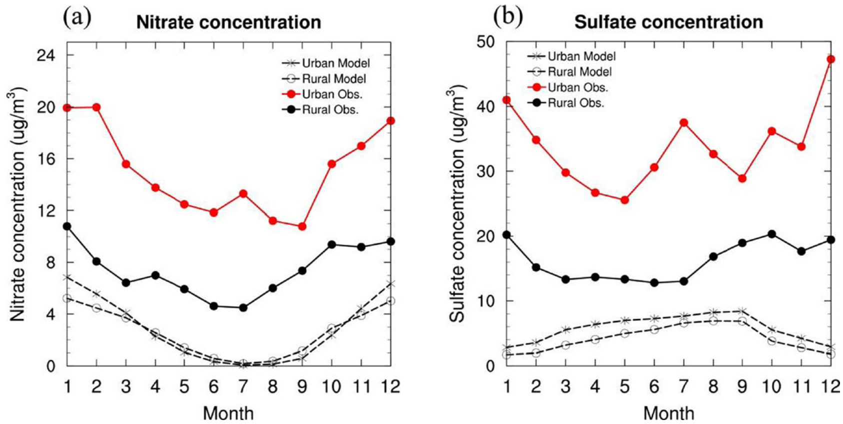

Fig. 11 Seasonal cycle of NCAR CAM-Chem simulated (interpolated to observational sites) and observed **a** nitrate and **b** sulfate surface concentrations (μg m^{-3}) in China. The *solid* and *dashed lines* are for the observed and model values, respectively. The details about these observation sites are referred to Zhang et al. (2012a)

3.5 Uncertainty of nitrate loading in China

The simulated summer nitrate loading is quite weak (less than 0.3 mg m^{-2}) in East Asia (Fig. 9a). In fact, rapid industrialization leads to increases in anthropogenic emissions in China (Richter et al. 2005; Lu et al. 2010). Here, we use an intensity index (Si) to describe the intensity of seasonal change in the decade of 2000s. The value of Si is determined by the formula,

$$\mathrm{Si} = \mathrm{abs}\left(\frac{V_{\max} - V_{\min}}{V_{\min}}\right),$$

where $V_{\max}$ and $V_{\min}$ are the maximum and minimum values, respectively, for a 12-month time series of nitrate loading. The Si for simulated nitrate loading in the 2000s is 24.02, 4.58, and 17.78 in East Asia, Europe, and North America, respectively. Meanwhile, the Si for simulated sulfate loading is only 1.58, 4.14, and 2.42 in the same regions, respectively. This indicates that the simulated seasonal variation of nitrate mass is quite strong in East Asia. Bellouin et al. (2011) and Lamarque et al. (2012) showed that the simulated surface layer nitrate mass concentrations agreed reasonably well with the observed concentrations in North America. However, a similar comparison in China has not been conducted due to sparse in situ measurements. Hence, we use surface mass concentrations from the Chinese aerosol network (Zhang et al. 2012a) to evaluate nitrate and sulfate mass concentrations used in this work. These measurements were taken during 2006–2007 at seven rural and seven urban sites. Figure 11 shows the seasonal changes in NCAR CAM-Chem simulated and observed concentrations of nitrate and sulfate aerosols at rural and urban sites. Based on observations, maximum mass concentrations of both nitrate and sulfate occur in winter, and there is also a second peak in summer for sulfate concentration at urban sites. These observed concentrations at urban sites are apparently higher than those at rural sites. With respect to the simulated concentrations from the NCAR CAM-Chem, the largest nitrate and sulfate concentrations are in January and October. The simulated concentrations are much lower than the measured values at urban sites but agree relatively close to measurements at rural sites. The underestimation of nitrate concentrations is the most serious in summer. The simulated seasonal cycles of surface layer nitrate and sulfate are stronger than those observed. For example, the seasonal intensity (Si) values are 1.40 and 0.85 for the observed nitrate and sulfate concentrations at rural sites, respectively, but the

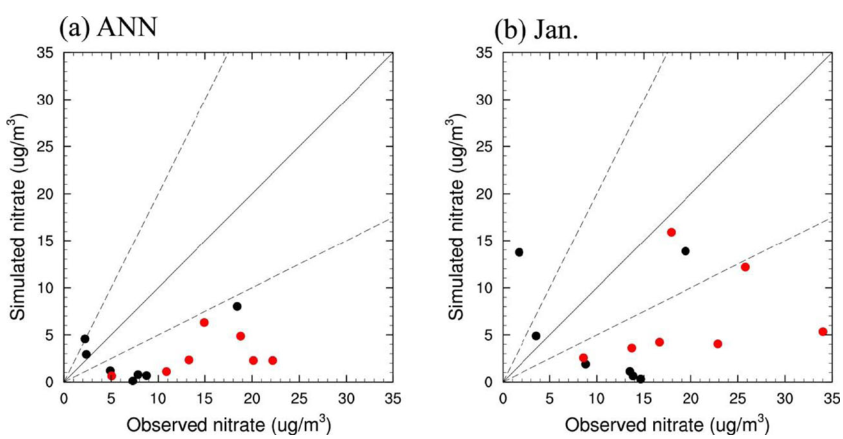

Fig. 12 Simulated (interpolated to observational sites) and observed surface nitrate concentration (μg m^{-3}) in China. **a**, **b** Are for the annual and January mean, respectively. The *black* and *red circles* denote rural and urban sites, respectively. Note: the 1:1 line is shown as a *solid line*; 1:2 and 2:1 lines are shown as *dashed lines*

corresponding Si increases to 27.72 and 1.98 in simulated concentrations. Besides, the seasonal variation of simulated sulfate is opposite to the observation.

According to the scatter plots shown in Fig. 12, nitrate concentrations are substantially underestimated in China, especially over urban regions. The observed nitrate concentrations are roughly half of the observed sulfate levels (Fig. 11), and the simulation does not well describe the ratios between the two aerosols. Considering the eastern transport of aerosols from eastern China, similar concentration underestimations may extend over many adjacent East Asian regions. As a result, our calculated AOD due to anthropogenic aerosols is very likely also underestimated over East Asia. Actually, some recent work (Liu et al. 2012; Shindell et al. 2013) shows that the AOD values in eastern China simulated by many climate models are smaller than the observations. Although the underestimation of total AOD also comes from other aerosols, both of sulfate and nitrate are key aerosol species in eastern China (Zhang et al. 2012a, b; Sun et al. 2014). Thus, many current climate models including our AGCM may further underestimate aerosol AOD and associated DRF in East Asia. In our study, the underprediction for simulated nitrate and sulfate aerosols is likely caused by inaccurate local emissions in China, given that the same model can obtain basically plausible results for Europe and North America (Lamarque et al. 2012). Wang et al. (2010) and Zhang et al. (2012b) obtained relatively higher nitrate DRF than our estimation in eastern China using some nitrate emissions in China. This further indicates that extensive efforts from scientific community are still required to improve the simulation of aerosol characteristics in East Asia in future studies.

4 Conclusion and discussion

The nitrate DRF and possible time evolution have been investigated in this study using the aerosol dataset simulated from the NCAR chemical transport model and meteorological fields from the LASG/IAP AGCM. Our focal points are on East Asia.

The present global annual mean anthropogenic nitrate DRF and its normalized value are calculated to be −0.025 W m^{-2} and −167 W g^{-1}, respectively. Meanwhile, stronger nitrate DRF occurs at industrialized regions in the Northern Hemisphere, especially in East Asia. The global mean anthropogenic nitrate loading and resulting DRF show a remarkable increase since the 1950s and will very likely increase to higher levels under future scenarios. Meanwhile, the global mean ratios of nitrate loading and DRF to anthropogenic aerosol species are gradually increasing, and the increasing trend could last. The global mean anthropogenic nitrate DRF by the end of the 21st century is estimated to be −0.039 and −0.049 W m^{-2} under RCP6.0 and RCP8.5, respectively, much higher than the present level and the middle-range RCP4.5 scenario (−0.025 W m^{-2}). This is quite different to anthropogenic sulfate loading and the corresponding DRF, which are even projected to decrease to the PI levels by 2100 at both the global and regional scales.

Our results further show that projected anthropogenic DRF due to nitrate aerosol in most regions may keep increasing except for some European and North American regions. In particular, the anthropogenic nitrate loading and corresponding DRF in East Asia exceed those in Europe and North America since the 1980s and are projected to continue to increase until the middle of the 21st century. The ratio of nitrate all-sky DRF to total anthropogenic aerosols is even projected to reach 60 % in East Asia. Our results therefore indicate that nitrate will play more and more important roles in the aerosol RF and even be the largest contributor to anthropogenic aerosol DRF over East Asia by the end of the 21st century. Moreover, the worst scenario for East Asia is RCP6.0, under which its peak time is the 2050s, when the maximum local DRF is estimated to be up to −2.0 W m^{-2} relative to the PI.

In addition, the simulated meteorological RH and clouds, which show distinct regional features, have important roles in determining the DRF of hydrophilic nitrate. This can partly explain the differences in the seasonal cycle of nitrate DRF in major industrialized regions. Nevertheless, the largest uncertainty is the nitrate atmospheric loading of nitrate, especially in East Asia. Compared to surface measurements in China, the simulated nitrate surface concentrations are much weaker, especially in summer, which likely result in weaker nitrate DRF. In addition, the simulated nitrate (and sulfate) especially over urban sites shows different seasonal variations when compared with measurements. It is then suggested that present chemical transport models should use more realistic East Asian emission dataset. More available relevant observations are also urgently expected to investigate and evaluate aerosol effects in East Asia. Nitrate aerosol has fine, accumulation and coarse modes and generally is internally mixed with other aerosols. Due to the limits of dataset and methods, we only considered nitrate with the bulk distribution and externally mixing treatment, which certainly will quantitatively influence the calculated nitrate DRF. Moreover, it should be noted that the aerosol concentrations and their radiative forcing are fully coupled with climate (Liao et al. 2009); future estimation of aerosol DRF should be conducted in an interactive climate model.

Acknowledgments This research was supported jointly by the National Basic Research Program of China (Grant Nos. 2013CB955803 and 2012CB955303) and the Office of Biological and Environmental Sciences, USA Department of Energy (grant to SUNYA). The authors would like to thank Dr. Lamarque of the NCAR for providing the NCAR CAM-Chem aerosol mass dataset.

References

Adams PJ, Seinfeld JH, Koch D, Mickley L, Jacob D (2001) General circulation model assessment of direct radiative forcing by the sulfate-nitrate-ammonium-water inorganic aerosol system. J Geophys Res 106(D1):1097–1111

Bao Q, Lin PF, Zhou TJ et al (2013) The Flexible Global Ocean–Atmosphere-Land system model, Spectral Version 2: FGOALS-s2. Adv Atmos Sci 30(3):561–576

Bauer SE, Koch D, Unger N, Metzger SM, Shindell DT, Streets DG (2007) Nitrate aerosols today and in 2030: a global simulation including aerosols and tropospheric ozone. Atmos Chem Phys 7:5043–5059

Bellouin N, Rae J, Jones A, Johnson C, Haywood J, Boucher O (2011) Aerosol forcing in the Climate Model Intercomparison Project (CMIP5) simulations by HadGEM2-ES and the role of ammonium nitrate. J Geophys Res 116(D20):D20206. doi:10.1029/2011JD016074

Chou MD (2002) Parameterization of shortwave cloud optical properties for a mixture of ice particle habits for use in atmospheric models. J Geophys Res 107:4600. doi:10.1029/2002JD002061

Edwards JM, Slingo A (1996) A studies with a flexible new radiation code. I: choosing a configuration for a large-scale model. Q J R Meteorol Soc 122:689–720

Fitzgerald JW (1975) Approximation formulas for the equilibrium size of an aerosol particle as a function of its dry size and composition and the ambient relative humidity. J Appl Meteorol 14:1044–1049

Folini D, Wild M (2011) Aerosol emissions and dimming/brightening in Europe: sensitivity studies with ECHAM5-HAM. J Geophys Res 116:D21104. doi:10.1029/2011JD016227

Forster P, Ramaswamy V, Artaxo P et al (2007) Changes in atmospheric constituents and in radiative forcing. In: Climate change 2007: the physical science basis. Contribution of Working Group I to the Fourth Assessment Report of the Intergovernmental Panel on Climate Change. Cambridge University Press, Cambridge, United Kingdom, and New York, NY, USA

Fu Q, Liou KN (1992) On the correlated *k*-distribution method for radiative transfer in nonhomogeneous atmospheres. J Atmos Sci 49:2139–2156

Haywood JM, Ramaswamy V (1998) Global sensitivity studies of the direct radiative forcing due to anthropogenic sulphate and black carbon aerosols. J Geophys Res 103:6043–6058

He B, Bao Q, Li J et al (2013) Influences of external forcing changes on the summer cooling trend over East Asia. Clim Change 117:829–841

Hess M, Koepke P and Schult I (1998) Optical properties of aerosols and clouds: The software package OPAC. Bull Am Meteorol Soc 79: 831–844

Hu YX, Stamnes K (1993) An accurate parameterization of the radiative properties of water clouds suitable for use in climate models. J Clim 6:728–742

Kiehl JT, Schneider TL, Rasch PJ, Barth MC, Wong J (2000) Radiative forcing due to sulfate aerosols from simulations with the National Center for Atmospheric Research Community Climate Model Version 3. J Geophys Res 105(D1):1441–1457

Lamarque JF, Kyle GP, Meinshausen M et al (2011) Global and regional evolution of short-lived radiatively-active gases and aerosols in the Representative Concentration Pathways. Clim Change 109:191–212

Lamarque JF et al (2012) CAM-chem: description and evaluation of interactive atmospheric chemistry in the Community Earth System Model. Geosci Model Dev 5:369–411

Li J, Barker HW (2005) A radiation algorithm with correlated *k*-distribution. Part I: local thermal equilibrium. J Atmos Sci 62:286–309

Li J, Wong JGD, Dobbie JS, Chylek P (2001) Parameterization of the optical properties of sulfate aerosols. J Atmos Sci 58:193–209

Li Z, Lee KH, Xin J, Wang Y, Hao WM (2010) First observation-based estimates of cloud-free aerosol radiative forcing across China. J Geophys Res 115:D00K18. doi:10.1029/2009JD013306

Li JD, Sun Z, Liu YM, Li JN, Wang WC, Wu GX (2012) A study on sulfate optical properties and direct radiative forcing using LASG-IAP general circulation model. Adv Atmos Sci 29(6):1185–1199

Liao H, Seinfeld JH (2005) Global impacts of gas-phase chemistry-aerosol interactions on direct radiative forcing by anthropogenic aerosols and ozone. J Geophys Res 110:D18208. doi:10.1029/2005JD005907

Liao H, Seinfeld JH, Adams PJ, Mickley LJ (2004) Global radiative forcing of coupled tropospheric ozone and aerosols in a unified general circulation model. J Geophys Res 109:D16207. doi:10.1029/2003JD004456

Liao H, Zhang Y, Chen WT, Raes F, Seinfeld JH (2009) Effect of chemistry-aerosol-climate coupling on predictions of future climate and future levels of tropospheric ozone and aerosols. J Geophys Res 114:D10306. doi:10.1029/2008JD010984

Liu X, Easter RC, Ghan SJ et al (2012) Toward a minimal representation of aerosols in climate models: description and evaluation in the Community Atmosphere Model CAM5. Geosci Model Dev 5: 709–739

Lu Z, Streets DG, Zhang Q et al (2010) Sulfur dioxide emissions in China and sulfur trends in East Asia since 2000. Atmos Chem Phys 10: 6311–6331

Martin G, Ringer M, Pope V, Jones A, Dearden C, Hinton T (2006) The physical properties of the atmosphere in the new Hadley Centre Global Environmental Model (HadGEM1). Part I: model description and global climatology. J Clim 19(7):1274–1301

Mlawer EJ, Taubman SJ, Brown PD, Iacono MJ, Clough SA (1997) Radiative transfer for inhomogeneous atmospheres: RRTM, a validated correlated-*k* model for the longwave. J Geophys Res 102(D14):16663–16682

Myhre G, Shindell D, Bréon F-M et al (2013a) Anthropogenic and natural radiative forcing. In: Stocker TF, Qin D, Plattner G-K, Tignor M, Allen SK, Boschung J, Nauels A, Xia Y, Bex V, Midgley PM (eds) Climate change 2013: the physical science basis. Contribution of Working Group I to the Fifth Assessment Report of the Intergovernmental Panel on Climate Change. Cambridge University Press, Cambridge

Myhre G, Samset BH, Schulz M et al (2013b) Radiative forcing of the direct aerosol effect from AeroCom Phase II simulations. Atmos Chem Phys 13(4):1853–1877

Pathak RK, Yao XH, Chan CK (2004) Sampling artifacts of acidity and ionic species in PM2.5. Environ Sci Technol 38:254–259

Richter A, Burrows JP, Nuss H, Granier C, Niemeier U (2005) Increase in tropospheric nitrogen dioxide over China observed from space. Nature 437(7055):129–132

Schaap M, Loon MV, ten Brink HM, Dentener FJ, Builtjes PJH (2004) Secondary inorganic aerosol simulations for Europe with special attention to nitrate. Atmos Chem Phys 4:857–874

Schulz M, Textor C, Kinne S et al (2006) Radiative forcing by aerosols as derived from the AeroCom present-day and pre-industrial simulations. Atmos Chem Phys 6:5225–5246

Shindell DT, Lamarque JF, Schulz M et al (2013) Radiative forcing in the ACCMIP historical and future climate simulations. Atmos Chem Phys 13(6):2939–2974

Skeie RB, Berntsen TK, Myhre G et al (2011) Anthropogenic radiative forcing time series from pre-industrial times until 2010. Atmos Chem Phys 11:11827–11857

Smith SJ, Aardenne JV, Klimont Z, Andres RJ, Volke A, Arias SD (2011) Anthropogenic sulfur dioxide emissions: 1850–2005. Atmos Chem Phys 11(3):1101–1116

Sun Z (2011) Improving transmission calculations for the Edwards–Slingo radiation scheme using a correlated-k distribution method. Q J R Meteorol Soc 137(661):2138–2148

Sun Z, Rikus L (1999) Improved application of ESFT to inhomogeneous atmosphere. J Geophys Res 104:6291–6303

Sun YL, Jiang Q, Wang ZF et al (2014) Investigation of the sources and evolution processes of severe haze pollution in Beijing in January 2013. J Geophys Res 119:4380–4398. doi:10.1002/2014JD021641

Takemura T (2012) Distributions and climate effects of atmospheric aerosols from the preindustrial era to 2100 along Representative Concentration Pathways (RCPs) simulated using the global aerosol model SPRINTARS. Atmos Chem Phys 12(23):11555–11572

Takemura T, Nakajima T, Dubovik O, Holben BN, Kinne S (2002) Single scattering albedo and radiative forcing of various aerosol species with a global three-dimensional model. J Clim 15:333–352

Taylor KE, Stouffer RJ, Meehl GA (2012) An overview of CMIP5 and the experiment design. Bull Am Meteorol Soc 93(4):485–498

Toon OB, Pollack JB, Khare BN (1976) The optical constants of several atmospheric aerosol species: ammonium sulfate, ammonium oxide and sodium chloride. J Geophys Res 81:5733–5748

Vuuren DP, Edmonds J, Kainuma M et al (2011) The representative concentration pathways: an overview. Clim Change 109:5–31

Wang T, Li S, Shen Y, Deng J, Xie M (2010) Investigations on direct and indirect effect of nitrate on temperature and precipitation in China using a regional climate chemistry modeling system. J Geophys Res 115:D00K26. doi:10.1029/2009JD013264

Wu G, Liu YM, He B et al (2012) Thermal controls on the Asian summer monsoon. Sci Rep 2:404. doi:10.1038/srep00404

Xu L, Penner JE (2012) Global simulations of nitrate and ammonium aerosols and their radiative effects. Atmos Chem Phys 12(20):9479–9504

Zhang XY, Wang YQ, Niu T et al (2012a) Atmospheric aerosol compositions in China: spatial/temporal variability, chemical signature, regional haze distribution and comparisons with global aerosols. Atmos Chem Phys 12(2):779–799

Zhang H, Shen Z, Wei X, Zhang M, Li Z (2012b) Comparison of optical properties of nitrate and sulfate aerosol and the direct radiative forcing due to nitrate in China. Atmos Res 113:113–125

Zhang H, Wang ZL, Wang ZZ et al (2012c) Simulation of direct radiative forcing of aerosols and their effects on East Asian climate using an interactive AGCM-aerosol coupled system. Clim Dyn 38:1675–1693